Real-Time Robotic Force Control for Automation of Ultrasound Scanning

Ungku Muhammad Zuhairi Ungku Zakaria, Seri Mastura Mustaza*,
Mohd Hairi Mohd Zaman, Ashrani Aizzuddin Abd Rahni
Department of Electrical-Electronic and Systems Engineering-Faculty of Engineering and Built Environment,
Universiti Kebangsaan Malaysia, 43600 UKM Bangi, Selangor Darul Ehsan, Malaysia

***Abstract*—Ablation represents a minimally invasive option for liver cancer treatment, commonly guided by imaging techniques such as ultrasound. Recently, there has been a surge in interest in semi-automated or fully automated robotic image acquisition. Specifically, there is a continuing interest in automating medical ultrasound image acquisition due to ultrasound being widely used, having a lower cost, and being more portable than other imaging modalities. This study explores automated robot-assisted ultrasound imaging for liver ablation procedures. The study proposed utilizing a collaborative robot arm from Universal Robots (UR), which has gained popularity across various medical applications. A robotic real-time force control system was designed and demonstrated to regulate the contact force exerted by the robot on the surface of a torso phantom, ensuring optimal contact during ultrasound imaging. The Robot Operating System (ROS) and the UR Real-Time Data Exchange (UR-RTDE) interface were employed to control the robot. The findings indicate that the contact force can be maintained around a set desired value of 9N. However, deviations occur due to residual forces from acceleration when the probe is not in contact with the phantom. These results provide a foundation for further advancements in the automation of ultrasound scanning.**

***Keywords*—Real-time; position control; force control; ROS; collaborative robot; admittance control; kinematics; dynamic; tool center point; damping**

I. INTRODUCTION

Ablation is a well-accepted minimally invasive procedure for treating certain cancerous tumors, especially in the case of liver cancer [1]. In ablation, image guidance is necessary during the procedure, such as using ultrasound and computed tomography (CT) fluoroscopy [2]. Navigation of the ablation needle is often performed manually under the expert guidance of the clinician and is operator-dependent. However, in some cases where there are not enough trained specialists, the radiologist may have to perform both the ablation procedure and ultrasound scanning simultaneously [24].

There is an increasing interest in automating the acquisition of medical ultrasound images due to its widespread use, cost-effectiveness, and portability compared to other imaging modalities. One promising approach involves using robotic arms, initially focused on remote ultrasonography or tele-imaging. Recently, attention has shifted towards semi-automated and fully automated robotic image acquisition systems. Hennersperger et al. [3] developed an innovative robotic ultrasound system utilizing the LBR iiwa robot. This system can autonomously execute imaging trajectories based on start and end points pre-selected by a physician in pre-interventional images such as MRI or CT scans. The trajectory is calculated by identifying the nearest surface point within the MRI data and integrating it with the corresponding surface normal direction to ensure accurate imaging. Von Haxthausen et al. [4] advanced this field by developing a system that, after the initial manual placement of the ultrasound probe, uses convolutional neural networks (CNNs) to control the robot and follow peripheral arteries. This integration of CNNs allows the system to adapt to complex anatomical variations and dynamically adjust the probe position, enhancing the precision and efficacy of the ultrasound imaging process. These advancements illustrate the potential of robotic systems to improve the accuracy and efficiency of medical ultrasound procedures. Using a robot arm to assist in ultrasound scanning frees the physician to focus on the ablation procedure. The robot arm end effector or gripper holds and manipulates the ultrasound probe to perform scanning during the ablation procedure [5]. The robot arm must have a range of motion for a full abdomen examination. At the same time, the force applied by the robot arm should be optimal for obtaining the best ultrasound images without causing any injury to the patient [6] [7]. Furthermore, fine-tuning the ultrasound probe position is also a requirement for the robot-assisted system to mimic human radiologists [8] [9].

This paper presents the development of a robotic ultrasound scanning system designed to fully replace sonographers, addressing a critical challenge faced by radiologists who simultaneously perform both ablation and ultrasound scanning. The introduction of robotic arms for ultrasound scanning allows medical practitioners to concentrate exclusively on ablation procedures, thereby enhancing their ability to deliver precise and effective treatment. Medical practitioners who multitask and perform both ablation and ultrasound scanning have difficulty handling and positioning the ultrasound probe during ultrasound scanning while doing ablation simultaneously. The implementation of robotic automated ultrasound scanning not only ensures consistent precision in imaging but also alleviates the complexities of manually handling and positioning the ultrasound probe during dual-task procedures. In employing robot arm replacing the sonographer, the automated robotic ultrasound scanning can be implemented.

This paper introduces a novel approach with real-time force control integrated into the robotic system based on Universal Robots (UR10e). The force control is particularly tailored for dynamic environments, utilizing an admittance control strategy

that responds to feedback forces. This approach ensures compliant force control, crucial for detecting and mitigating excessive force applied during scanning. Additionally, the consideration of damping in the admittance control strategy further enhances force accuracy and prioritizes patient safety during the scanning process. For hardware, the robot arm UR10e was used for the apparatus of ultrasound scanning. The custom gripper was attached to UR10e's end-effector and used to grip the ultrasound probe. The mechanism and shape of the custom gripper also aid the robot in mimicking the exact angle and the point for scanning the human body. The real-time force control was done similar to the point of scanning on the body and the angle of the real sonographer during ultrasound scanning.

The subsequent sections are structured as follows: Section II presents a comparison of the literature review. Section III outlines the methodology for hardware and software setup, as well as their integration for seamless operation. In Section IV, the findings from conducting robotic automated ultrasound scanning are detailed, along with an analysis of the results. Lastly, Section V offers conclusions and discusses future avenues of work.

II. Literature Review

Robot-assisted ultrasound scanning requires advanced and precise robot arm control [6], especially during an ablation procedure. In a typical system, a single robot arm holds and moves the ultrasound probe. The robot arm trajectory is initially planned in the pre-operative phase based on acquired CT or MRI images [6]. Advanced multimodal visualization is required for pre-operative image-based planning in this case. Forward kinematics can be computed to plan the robot arm trajectory based on Denavit-Hartenberg (D-H) parameters [10][5]. Two control methods have been used for gaining precise and accurate control for physical human-robot interaction, i.e., impedance control and admittance control [26]. For Impedance Control, the input gained is displacement or velocity, and the output is force. In vice versa, the Admittance Control input is force, and the output is displacement or velocity [27]. For this paper, the admittance control was implemented to set the amount of force desired and receive the feedback force from the contact so the robot would maintain the force value based on the amount of force selected.

Given the critical importance of contact force in ultrasound scanning, several recent studies have focused on ensuring constant contact force. Ulrich et al. [11] reported a mean contact force of 9 N with a peak force of 37 N during obstetric scanning. Similarly, Ning et al. [12] found a mean contact force of 8.5 N. In contrast, Chen et al. [13] recommended a lower contact force of 4.5 N for scanning the human body using Universal Robots (UR). Wang et al. [14] suggested initiating contact with a force of 15 N, subsequently maintaining it at 10 N for optimal imaging of the human spine. Kaminski et al. [15] proposed a target contact force of 7 N to ensure stable data acquisition. Meanwhile, Mohamed [16] established a reference range of 3-5 N for ultrasound scanning to balance probe stability and patient comfort. These varying recommendations highlight the need for context-specific force adjustments to enhance the precision and reliability of robotic ultrasound systems across different medical applications.

The duration of ablation procedures, particularly radiofrequency ablation (RFA), is a critical factor in their effectiveness and safety. Ma et al. [17] reported that the mean procedure time for ultrasound (US)-guided RFA is approximately 27.54 ± 12.06 minutes. In a study by Zeno et al. [18], the median duration of RFA was 14 minutes, ranging from 10 to 19.5 minutes. Over a decade-long study, Shuangyan et al. [19] found the median ablation time to be 26 minutes, extending from 12 to 120 minutes. Additionally, Zuo-Feng Xu et al. [20] observed that synchronizing US and CT images required an average of 13.9 ± 11.9 minutes, ranging from 5 to 55 minutes. They also noted that each individual or overlapping ablation session lasted approximately 12 minutes [20] [21]. In contrast, Wei et al. [22] reported a consistent ablation duration of 10 minutes per session. These findings highlight the variability in ablation times, which can be influenced by factors such as the imaging modality used, the complexity of the case, and the specific protocols of different medical centers. Understanding these timeframes is essential for optimizing procedure planning and improving patient outcomes.

III. Methodology

The hardware setup employed in this study will be comprehensively described, emphasizing the specific equipment and configurations utilized throughout the research. This includes detailed information on the types of hardware components and how they are integrated into the overall system. Subsequently, the software setup will be described, focusing on the software interfaces and implementation of software tools, as well as the software system's architecture. Finally, the force control mechanism will be thoroughly examined. This involves an in-depth discussion of the feedback control systems implemented to regulate the contact force applied by the robotic arm. The methodology for applying and adjusting the force over a specified duration will be detailed, including the algorithms and sensors used to achieve precise control.

A. Hardware Setup

The collaborative robot arm UR10e model from Universal Robots (UR) was chosen as the manipulator in handling the ultrasound probe to automate ultrasound scanning. Fig. 1 illustrates the hardware setup of the UR robot.

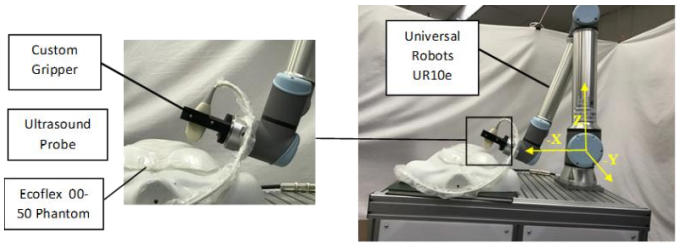

Fig. 1. (a) Hardware setup of ultrasound scanning (b) Hardware setup of the experiment with a coordinate system.

A partially rigid phantom was employed in this study to represent a human body. The anterior surface of the phantom is partially covered with cured Ecoflex 00-50 gel, a silicone gel that is commonly used for ultrasound phantoms [23]. As illustrated in Fig. 1(a), the robot is equipped with a custom gripper designed to handle an ultrasound probe. This probe

choice ensures that our experimental setup closely mirrors clinical practice, enhancing our findings' validity and applicability. The robot's coordinate system is as illustrated in Fig. 1(b). The origin coordinate is established at the base of the robot. The orientation was defined as Euler angles around each axis: θ = [θx θy θz]. Consequently, the robot's pose is represented as a 6-element vector comprising the 3D position, p = [x, y, z] (in meters), and the orientation, θ (in radians), forming the vector [x, y, z, θx, θy, θz]. The robot's end effector is equipped with a built-in force/torque sensor. This sensor is instrumental in measuring the external forces exerted by the phantom. The specifications of the built-in force/torque sensor are detailed in Table I, highlighting its range, precision, and accuracy.

TABLE I. SPECIFICATION OF BUILT-IN FORCE/TORQUE SENSOR IN UNIVERSAL ROBOT UR10E

Force sensing, tool flange/torque sensor	Force, x-y-z	Torque, x-y-z
Range	100.0N	10.0 Nm
Precision	5N	0.2 Nm
Accuracy	5N	0.5 Nm

B. Software Setup

Robot Operating System (ROS) is used in this work in a computer with Ubuntu operating system. The integration of UR dependencies facilitates the control of the UR robotic arm. This integration enables the robot to be managed by a computer, displaying the data acquired from the UR system. For real-time control, the UR Real-Time Data Exchange (UR-RTDE) libraries are being specifically utilized to harness the capabilities of the UR robot arm. Python was selected due to its robustness and extensive support for both ROS and UR-RTDE libraries to implement the ROS and UR-RTDE interface.

Fig. 2 illustrates the control architecture for the automation of ultrasound scanning. F_a represents the external contact force exerted to the probe, F_d represents the desired force, and F_e is the difference between them.

Admittance control was applied for this work. Robot admittance control models [25] [26] [27], were used to maintain the force value exerted during ultrasound scanning of the ablation process, mimicking the scan conducted by the sonographer. The control model is represented by the following equation:

$$F_e(\tau) = F_a(\tau) - F_d(\tau)$$

$$F_e(\tau) = \mathrm{M}(x\blacklozenge(\tau) - \ddot{x}_d(\tau)) + \Delta\,(x(\tau) - \dot{x}_d(\tau)) + \mathrm{K}\,(x(\tau)\,x_d(\tau)) \quad (1)$$

where, M is virtual mass, D is damping and K is stiffness coefficient. x_d denotes the desired position of the tip of the robot, while x is the position, $\dot{x}$ is the velocity and $\ddot{x}$ is the acceleration. The admittance control model is applied across each degree of freedom. However, our focus can only be directed towards the degrees of freedom along the x-axis- and z-axis.

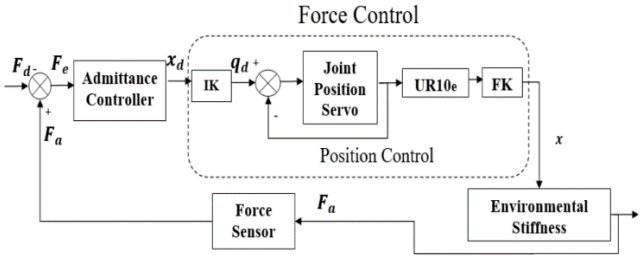

Fig. 2. Block diagram of force control system.

Based on Eq. (1), the admittance parameters can be adjusted to achieve specific dynamic characteristics of the robot system in the presence of external forces, i.e., from the patient or a static phantom. Phantom is only static. Therefore, M and K have been set as fixed values. So, D will be adjusted and controlled. For the UR force control interface, the range of the damping parameter can be set from 0 to 1, which the default value of the damping parameter is 0.005. The higher the value, the greater the deceleration during exerted force, and vice versa [28]. Deceleration is required to reduce force overshoot, thus reducing excessive force. Hence, an evaluation comparison of the damping factor was conducted to choose the best value. Four damping factors were compared: 0.005, 0.01, 0.02, and 0.05.

Referring to Fig. 2, the input force F_e, the difference between F_a and F_d, was applied to the admittance control, which resulted in moving to the displacement desired, x_d. Next, the inverse kinematics of the robot, IK, received input, x_d, and produce output, q_d to move the joint in position control closed loop. Afterward, forward kinematics of the robot, FK releases the output x to the environmental stiffness, which is the phantom resulting in the contact force, F_a. The force sensor will detect the value of F_a, and then send the value to be compared with the desired force input F_d, which resulting force input F_e.

To verify the efficiency of force control, including admittance control, a comparison between position control and overall force control was made to choose which control system is the best for full robotic automated ultrasound scanning. Three conditions were tested for evaluation, which are a slow movement with an acceleration of 0.1 ms^{-2}, fast movement with acceleration of 2 ms^{-2} and in a static position.

C. System Integration

Integration of hardware and software setup has been made for force control. A full operation of force can be achieved by satisfying a force overshoot capability involving position function, as shown in Fig. 3.

Referring to Fig. 3, the robot arm operates based on commands issued from the computer. The force is detected on the Tool Center Point (TCP) that has been set. To apply force, the position of the end-effector changes toward the direction of the force applied. Once the force sensor detects the external force, the measured force value is transmitted to the computer. When there is a deviation between the measured force and the desired force value, the computer processes this information and sends corrective commands to the robot to maintain the desired force during operation.

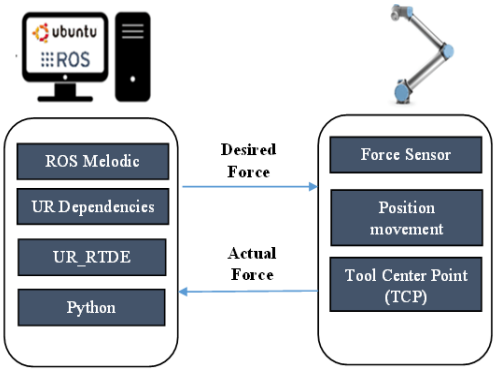

Fig. 3. Full setup of a system.

Using the UR-RTDE interface, the initial pose first needs to be set. The initial pose that has been set for this work is [-0.5, -0.1, 0.15, 0, 70/180 π, 0]. The pose can be seen in Fig. 4, along with the original and new Tool Point Center (TCP) of the robot, which is [0, -0.055, 0.058, 0, 0, 0] (green). This change is to ensure the accuracy of choosing a better coordinate for scanning. This new TCP has been set, and the pose coordinates were referred to at the end of the probe.

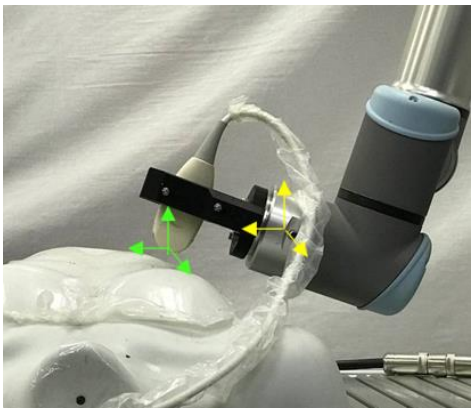

Fig. 4. Original TCP (Yellow) and New TCP (Green).

As illustrated in Fig. 5, the force task frame was set to [0, 0, 0, 0, 1.0472, 0] for the force to be exerted at 1.0472 radian pointing towards the phantom due to mimicking the liver position of the human.

When the configuration above is completed, the experiment has been done. The damping factor values have been evaluated, and the suitable values have been chosen. A comparison of position control and force control was also conducted to ensure the most compatible control system. After those evaluations have been executed, force control can be conducted. 9N was chosen based on the obstetric median force value [11], and 9N must be maintained when the force is exerted on the phantom. This work is set for 12 minutes during the exertion of force based on the time taken for ultrasound scanning conducted [20] [21]. The process flow of this experiment is shown in Fig. 6.

According to Fig. 6, the robot end-effector will first move to the initial position. Subsequently, a force is applied. If the detected force deviates from 9N, the robot will adjust to maintain a force of 9N. Upon achieving a stable force of 9N, the robot will operate for a duration of 12 minutes. Throughout this period, the force of 9N will be consistently maintained until the 12-minute mark is reached. Once the 12 minutes have elapsed, the robot end-effector will return to the initial position, concluding the process.

Fig. 5. Force task frame of the robot.

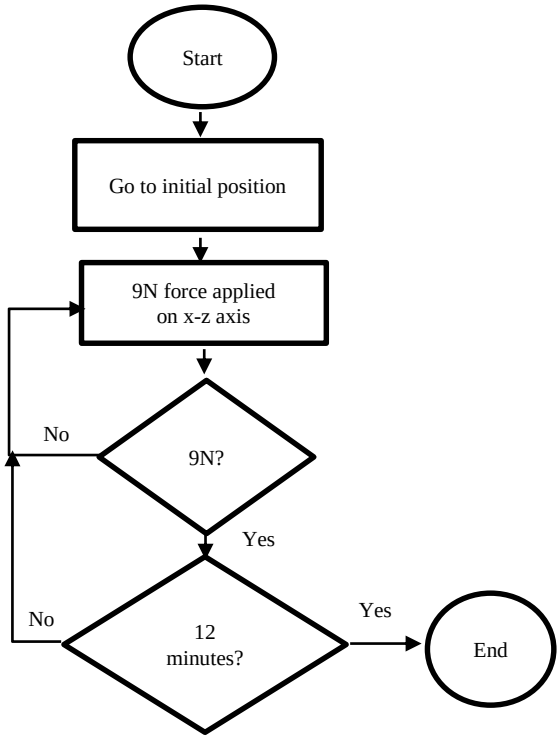

Fig. 6. Flowchart of the force control experiment.

IV. Results and Discussions

The experiment was conducted based on the setup that have been made. Firstly, the evaluation of damping factor values was conducted. Subsequently, a comparison of position and force control was made involving admittance control. Finally, force control of robotic automated ultrasound scanning was performed to appraise force retention over a certain amount of time.

The damping factor was evaluated to determine the most suitable overshoot for applying the force. Four damping values were selected, and the corresponding forces were measured. Additionally, a comparative analysis was conducted between position control and force control. Initially, the force was measured using position control alone. Subsequently, force control was implemented using the damping factor value selected from the prior comparison.

After evaluating the damping factor and the suitable control for applying force to the phantom, the force control was conducted for 12 minutes to evaluate the consistency of the force, which is 9N.

A. Evaluation of Damping Factor

Experimental testing was carried out to characterize the damping and overshoot of the contact forces between the ultrasound probe attached to the UR robot and the phantom to investigate the performance of the force control system. The robot exerted a 9N force onto the phantom in this experiment for 12 seconds. The damping factor was systematically varied between 0.005 and 0.05, and the resulting contact forces between the ultrasound probe and the phantom were recorded, as well as the overshoot that occurred upon contact. The results of this experiment are shown in Fig. 7(a)-(d).

At a damping factor of 0.005, as illustrated in Fig. 7(a), the force overshoot initially peaks at 15N before stabilizing at 9N by the 4th second overshoot. When the damping factor is increased to 0.01, as shown in Fig. 7 (b), the force overshoot peaks between 10N and 15N and stabilizes at 9N by approximately the 3rd second overshoot. With a damping factor of 0.02, as depicted in Fig. 7 (c), the force overshoot shows stabilization at 9N shortly after the two seconds overshoot. Finally, at a damping factor of 0.05, shown in Fig. 7 (d), no force overshoot is observed, and 9N of force is applied just before the two seconds.

The percentage overshoot corresponding to each damping factor is tabulated in Table II. The percentage overshoot of the applied force at a damping factor of 0.005 is 61%. As the damping factor is increased to 0.01, the percentage overshoot decreases to 41%. Further increasing the damping factor to 0.02 results in a percentage overshoot of 26.55%. At a damping factor of 0.05, the percentage overshoot is completely eliminated, reaching 0%.

These observations demonstrate a clear inverse relationship between the damping factor and the percentage overshoot. Specifically, as the damping factor increases, the percentage overshoot of the applied force decreases correspondingly. This trend highlights the effectiveness of higher damping factors in achieving rapid stabilization of the force with minimal overshoot. Achieving zero overshoot at a damping factor of 0.05 indicates optimal damping, where the force control system can maintain the desired force precisely without any initial excess. This optimization is crucial for ensuring the reliability and accuracy of the ultrasound imaging process, as it minimizes the risk of excessive force application that could compromise image quality or cause damage to the phantom.

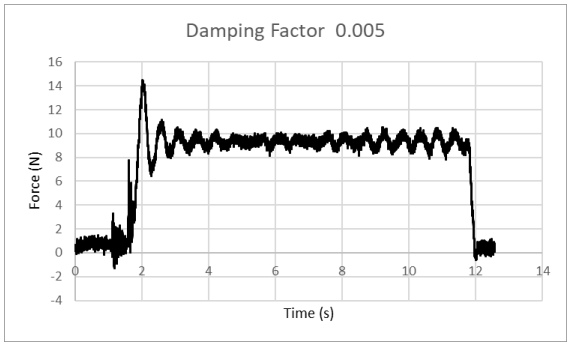

(a)

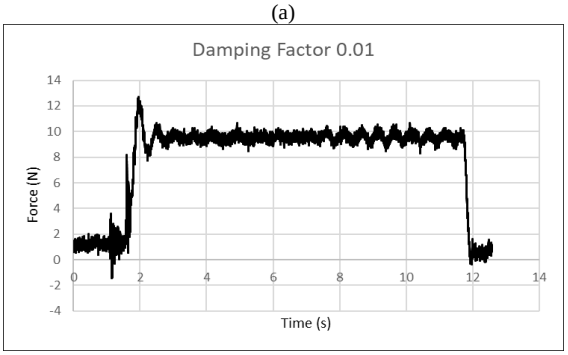

(b)

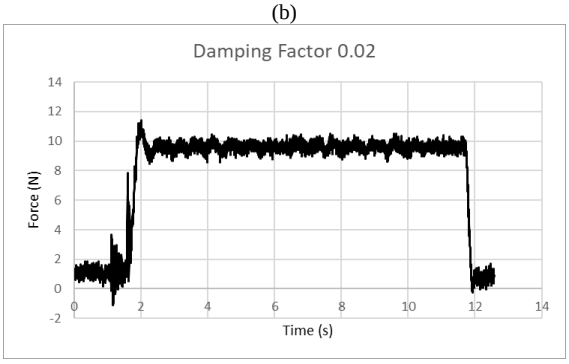

(c)

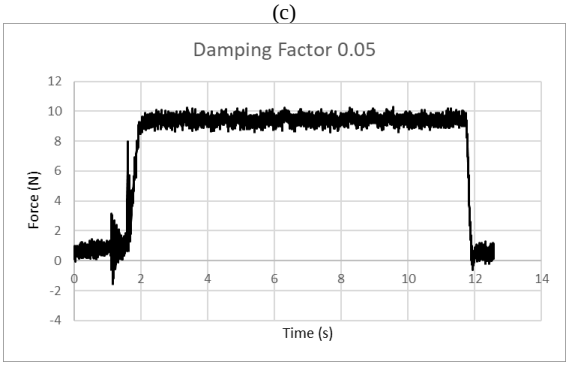

(d)

Fig. 7. The force value with damping factor (a) 0.005 (b) 0.01 (c) 0.02 (d) 0.05.

TABLE II. THE FORCE PERCENTAGE OVERSHOOT OF THE RESPECTIVE DAMPING FACTOR

Damping factor	Percentage overshoot (%)
0.005	61
0.01	41
0.02	26.55
0.05	0

B. Comparison of Positiom Control and Force Control

A comparative analysis between position control and force control was conducted to identify the most suitable method for applying force. Three conditions were examined to determine the optimal control strategy, which are 1) slow robot arm movement, 2) fast robot arm movement, and 3) static arm position. For the slow and fast movement condition, the ultrasound probe was controlled to move on and along the phantom stomach, starting from the liver towards the opposite side and returning to the liver position. For the slow movement, the robot arm drives the ultrasound probe at 0.1 ms^{-2} for 7 seconds, while for the fast movement, the acceleration is 2 ms^{-2} and the experiment runs for five seconds. The robot remained stationary at the liver area coordinates while contacting the phantom for the static condition. The comparison of position control and force control was plotted in Fig. 8 for slow movements, Fig. 9 for fast movement, and Fig. 10 for static position. 9N was set as the desired value to be achieved and was indicated with a horizontal line in Fig. 8, Fig. 9, and Fig. 10. The dashed line indicates position control, and the star line indicates force control.

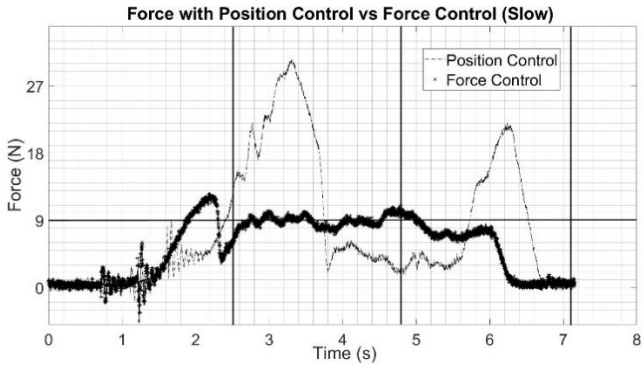

Fig. 8. Comparison of position control and force control in acceleration of 0.1 ms^{-2}.

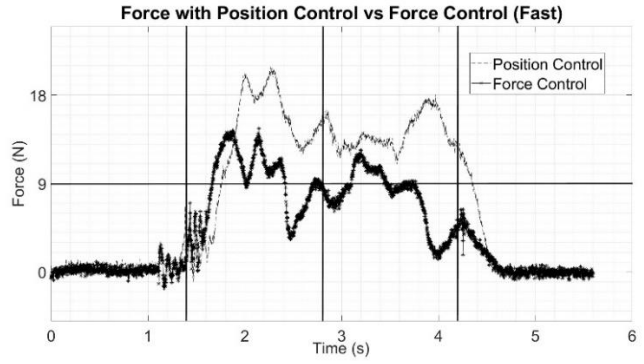

Fig. 9. Comparison of position control and force control in acceleration of 2 ms^{-2}.

Referring to Fig. 8, there are three lines in the graph that indicate the timeline of the position of the end-effector. The first line indicates the end-effector touching the phantom, which is 2.5 seconds; the second line is the movement from the liver to the stomach, which is 4.8 seconds; and the third line indicates the end-effector was returned to the liver part, which is 7.1 seconds. In the first line, the force in the position control is higher and has a huge difference compared to the force control below 9N. Upon reaching the second line, the force in the position control overshoots above 27N and drops drastically below 9N. Meanwhile, the force in the force control fluctuates close to 9N and tries to maintain the desired value, 9N. Finally, upon the march to the third line, the force in the position control overshoots again until above 18N and drops drastically. In contrast to force control, the force is very close to 9N, but eventually, the force value drops as it reaches the third line.

Based on Fig. 9, three vertical lines in the graph indicate the timeline of the end-effector's position. The first vertical line indicates the end-effector touching the phantom, which is at 1.4 seconds; the second line is the movement along the abdominal part, which is 2.8 seconds; and the third line indicates the return of the probe to the liver part, which is 4.2 seconds. In the first line, there were no significant differences in force between position control and force control. However, substantial differences exist in which the force in the control position was higher than the force in force control upon reaching the second line. Forces on both controls were turbulent. However, the force control is closer to 9N than the position control. Similar cases occurred from the second line to the third line in which the value of force in position control is greater than that in force control. After the graph's third line, the force value on both controls drops significantly.

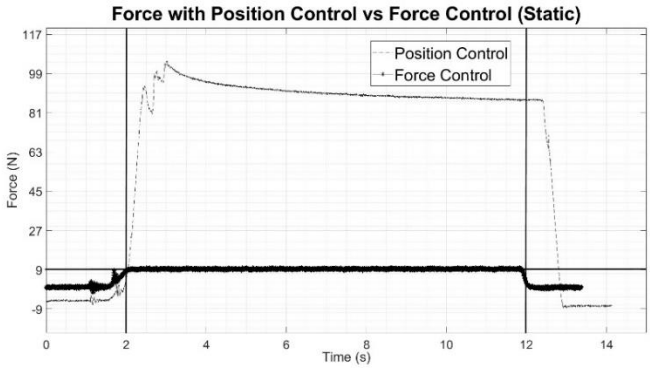

Fig. 10. Comparison of position control and force control in static position.

According to Fig. 10, two lines in the graph indicate the timeline of the end-effector's position. The first line indicates the end-effector touching the phantom, which is two seconds, and the second line is the position of the end-effector was lifted away from the phantom, which is 12 seconds. This graph illustrates the huge difference amount of force between position control and force control. On position control, the amount of force exceeds 100N and slightly decreases upon touching the phantom. However, it still overruns the desired amount of force, which is 9N. Contrarily, the force value in force control maintained 9N from the first line upon touching the phantom until the end effector was lifted away from the phantom. After the second line, the difference in force decrement was displayed. The value of force in force control dropped quickly compared to the force of the position control.

Based on the overall analysis, the amount of force in force control is closer to achieving the desired value than the position control, which is 9N. Even though there is a fluctuation of force value in Fig. 8 and Fig. 9 due to acceleration during movement and the curve surface of the phantom, the difference in the force

value from force control is lower compared to the position control. Meanwhile, in Fig. 10, the force control achieved and maintained the desired value of 9N compared to the position control, which exceeds the higher value.

It can be stated that using force control is more stable than using position control due to its closer adherence to the desired force value. When comparing acceleration, the force control method, with an acceleration of 0.1 ms^{-2}, proves to be the optimal control strategy. This is because lower acceleration results in lower force overshoot. The static condition experiment proves that the force control strategy employed is capable of maintaining the desired force value during its entire operation of 12 mins.

C. Operation of Force Control

Referring to the motion sequence described in Fig. 6, the resultant x-axis position, the resultant z-axis, and the magnitude of the force in the x-axis and z-axis, |Fxz| is shown in Fig. 11, Fig. 12, and Fig. 13 Firstly, the end effector will go to the initial position that has been set. Then, the robot will exert 9N on the phantom. The full operation of robotic force control was run for 12 minutes.

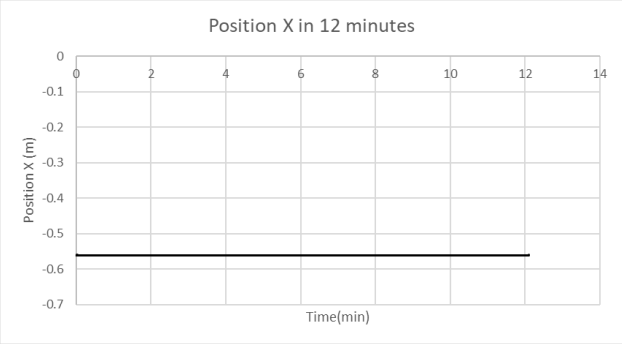

Fig. 11. x-axis position.

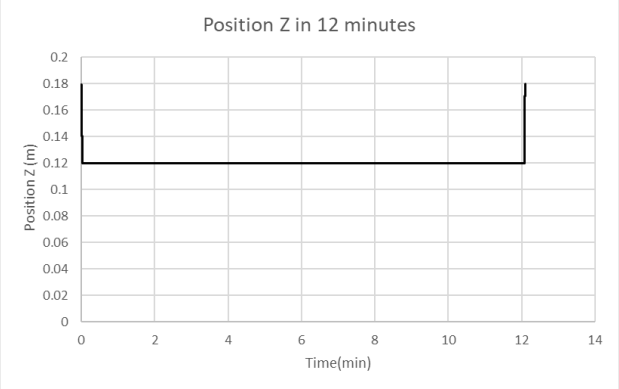

Fig. 12. z-axis position.

From Fig. 11 and Fig. 12, the x-axis and z-axis positions are at the initial position, which is pose x=-0.5m and pose z= 0.15m. Then, it suddenly changed due to the force direction towards the x and z direction. The force exerted can be seen in Fig. 10. From Fig. 13, no force is exerted when the end-effector is in the initial position. Then, the force of 9N is exerted upon touching the phantom. Next, the force was maintained at 9N along the operation. Even though there were light changes of force, the robot was able to maintain the force based on feedback until 12 minutes. This result, with a mean force of 9.503N and a standard deviation of 0.282N, corresponds to the force measured during abdominal scans in a previous study conducted by Ulrich and Struijk [11]. After 12 minutes, the x-axis and z-axis positions will return to the initial positions. Meanwhile, the force decreases drastically when the probe does not contact the phantom.

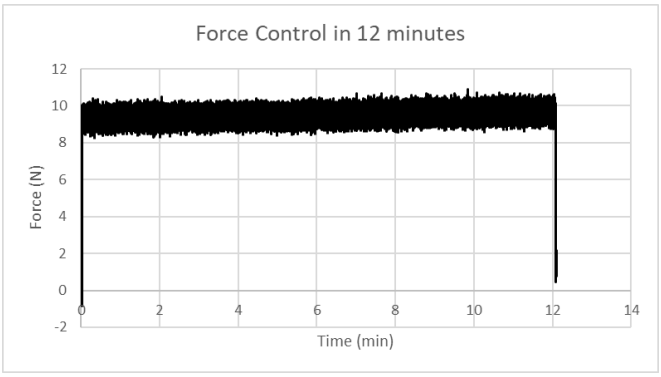

Fig. 13. Force along xz-axis,|Fxz|.

V. CONCLUSION

Ablation is a minimally invasive method for combating and eliminating liver cancer that involves crucial procedures such as ultrasound scanning. However, a single sonographer's simultaneous conduct of ablation can pose challenges. Hence, a proposal for robotic automated ultrasound scanning employing force control has emerged. Utilizing Universal Robot, the hardware and the corresponding software algorithm have been set up. Evaluation has been carried out, focusing on comparing damping factors and the efficacy of position control versus force control. It has been demonstrated that a damping value of 0.05 results in zero percentage overshoot. Furthermore, implementing force control ensures a more stable force than relying solely on position control. The full operation, lasting 12 minutes, maintains the desired force of 9N until its completion.

The real-time robotic force control was proven reliable in ultrasound scanning during liver ablation. The experiment above shows that contact force can be maintained around 9 N, albeit with deviation due to the residual force from acceleration when the probe is not in contact with the phantom. This shows that 9N can be applied on the phantom and, hence, on real ultrasound sonography. Furthermore, this paper can be used for further development of robot-assisted ultrasound scanning.

For future work, the cohesive gripper can be designed to be compatible with various types of ultrasound probes and robotic end-effectors, facilitating seamless attachment. The implementation of a compatible gripper is essential to maintain accuracy and efficiency during ultrasound scanning procedures.

Additionally, integrating image recognition technology with automation could enhance the system, allowing the robot to precisely identify the optimal location for performing ultrasound scans on the targeted area. This would eliminate the need for the patient to precisely position themselves against the surface where the robot is set to perform the ultrasound at a predetermined point.

ACKNOWLEDGMENT

The research is supported by research grant no. GUP-2021-024 and CRIM PIP-SH-2020-06 from Universiti Kebangsaan Malaysia.

REFERENCES

[1] D. Yang, L. Wang, Y. Xie, W. S. Levine, R. Davoodi, and Y. Li, "Optimization-based inverse kinematic analysis of an experimental minimally invasive robotic surgery system," in 2015 IEEE International Conference on Robotics and Biomimetics, IEEE-ROBIO 2015, Institute of Electrical and Electronics Engineers Inc., 2015, pp. 1427–1432. doi: 10.1109/ROBIO.2015.7418971.

[2] J. Schaible et al., "Primary efficacy of percutaneous microwave ablation of malignant liver tumors: comparison of stereotactic and conventional manual guidance," Sci Rep, vol. 10, no. 1, Dec. 2020, doi: 10.1038/s41598-020-75925-6.

[3] C. Hennersperger et al., "Towards MRI-Based Autonomous Robotic US Acquisitions: A First Feasibility Study," IEEE Trans Med Imaging, vol. 36, no. 2, pp. 538–548, 2017, doi: 10.1109/TMI.2016.2620723.

[4] F. Von Haxthausen, J. Hagenah, M. Kaschwich, M. Kleemann, V. García-Vázquez, and F. Ernst, "Robotized ultrasound imaging of the peripheral arteries - A phantom study," Current Directions in Biomedical Engineering, vol. 6, no. 1, pp. 1–4, 2020, doi: 10.1515/cdbme-2020-0033.

[5] X. Guan et al., "Study of a 6DOF robot assisted ultrasound scanning system and its simulated control handle," 2017 IEEE International Conference on Cybernetics and Intelligent Systems, CIS 2017 and IEEE Conference on Robotics, Automation and Mechatronics, RAM 2017 - Proceedings, vol. 2018-Janua, pp. 469–474, 2017, doi: 10.1109/ICCIS.2017.8274821.

[6] T. Y. Fang, H. K. Zhang, R. Finocchi, R. H. Taylor, and E. M. Boctor, "Force-assisted ultrasound imaging system through dual force sensing and admittance robot control," Int J Comput Assist Radiol Surg, vol. 12, no. 6, pp. 983–991, 2017, doi: 10.1007/s11548-017-1566-9.

[7] Y. Minami and M. Kudo, "Ultrasound fusion imaging of hepatocellular carcinoma: A review of current evidence," Digestive Diseases, vol. 32, no. 6, pp. 690–695, 2014, doi: 10.1159/000368001.

[8] N. Agarwal, A. K. Yadav, A. Gupta, and M. Felix Orlando, "Real-time needle tip localization in 2D ultrasound images using kalman filter," IEEE/ASME International Conference on Advanced Intelligent Mechatronics, AIM, vol. 2019-July, pp. 1008–1012, 2019, doi: 10.1109/AIM.2019.8868799.

[9] M. Renfrew, M. Griswold, and M. C. Çavuşoğlu, "Active localization and tracking of needle and target in robotic image-guided intervention systems," Auton Robots, vol. 42, no. 1, pp. 83–97, 2018, doi: 10.1007/s10514-017-9640-2.

[10] Y. Y. Cao et al., "Composite Configuration Interventional Therapy Robot for the Microwave Ablation of Liver Tumors," Chinese Journal of Mechanical Engineering (English Edition), vol. 30, no. 6, pp. 1416–1425, 2017, doi: 10.1007/s10033-017-0141-1.

[11] C. Ulrich and L. N. S. Andreasen Struijk, "Probe contact forces during obstetric ultrasound scans - A design parameter for robot-assisted ultrasound," Int J Ind Ergon, vol. 86, Nov. 2021, doi: 10.1016/j.ergon.2021.103224.

[12] G. Ning, J. Chen, X. Zhang, and H. Liao, "Force-guided autonomous robotic ultrasound scanning control method for soft uncertain environment," Int J Comput Assist Radiol Surg, vol. 16, no. 12, pp. 2189–2199, 2021, doi: 10.1007/s11548-021-02462-6.

[13] S. Chen, Z. Li, Y. Lin, F. Wang, and Q. Cao, "Automatic ultrasound scanning robotic system with optical waveguide-based force measurement," Int J Comput Assist Radiol Surg, vol. 16, no. 6, pp. 1015–1025, 2021, doi: 10.1007/s11548-021-02385-2.

[14] Y. Wang, T. Liu, X. Hu, K. Yang, Y. Zhu, and H. Jin, "Compliant Joint Based Robotic Ultrasound Scanning System for Imaging Human Spine," IEEE Robot Autom Lett, vol. 8, no. 9, pp. 5966–5973, Sep. 2023, doi: 10.1109/LRA.2023.3300592.

[15] J. T. Kaminski, K. Rafatzand, and H. Zhang, "Feasibility of robot-assisted ultrasound imaging with force feedback for assessment of thyroid diseases," SPIE-Intl Soc Optical Eng, Mar. 2020, p. 48. doi: 10.1117/12.2551118.

[16] M. E. Karar, "A Simulation Study of Adaptive Force Controller for Medical Robotic Liver Ultrasound Guidance," Arab J Sci Eng, vol. 43, no. 8, pp. 4229–4238, Aug. 2018, doi: 10.1007/s13369-017-2893-4.

[17] M. Luo et al., "Percutaneous ablation of liver metastases from colorectal cancer: a comparison between the outcomes of ultrasound guidance and CT guidance using propensity score matching," Ultrasonography, vol. 42, no. 1, pp. 54–64, Jan. 2023, doi: 10.14366/usg.21212.

[18] Z. Sparchez et al., "Percutaneous ultrasound guided radiofrequency and microwave ablation in the treatment of hepatic metastases. A monocentric initial experience.," Med Ultrason, vol. 21, no. 3, pp. 217–224, 2019, doi: 10.11152/mu-1957.

[19] S. Ou et al., "Radiofrequency ablation with systemic chemotherapy in the treatment of colorectal cancer liver metastasis: A 10-year single-center study," Cancer Manag Res, vol. 10, pp. 5227–5237, 2018, doi: 10.2147/CMAR.S170160.

[20] Z. F. Xu et al., "Percutaneous radiofrequency ablation of malignant liver tumors with ultrasound and CT fusion imaging guidance," Journal of Clinical Ultrasound, vol. 42, no. 6, pp. 321–330, 2014, doi: 10.1002/jcu.22141.

[21] J. Kang et al., "Comparative study of shear wave velocities using acoustic radiation force impulse technology in hepatocellular carcinoma: The extent of radiofrequency ablation," Gut Liver, vol. 6, no. 3, pp. 362–367, Jul. 2012, doi: 10.5009/gnl.2012.6.3.362.

[22] W. J. Fan, X. Li, L. Zhang, H. Jiang, and J. L. Zhang, "Comparison of microwave ablation and multipolar radiofrequency ablation in vivo using two internally cooled probes," American Journal of Roentgenology, vol. 198, no. 1, Jan. 2012, doi: 10.2214/AJR.11.6707.

[23] A. Cafarelli, P. Miloro, A. Verbeni, M. Carbone, and A. Menciassi, "Speed of sound in rubber-based materials for ultrasonic phantoms," J Ultrasound, vol. 19, no. 4, pp. 251–256, Dec. 2016, doi: 10.1007/s40477-016-0204-7.

[24] G. Laimer, P. Schullian, and R. Bale, "Stereotactic thermal ablation of liver tumors: 3d planning, multiple needle approach, and intraprocedural image fusion are the key to success—a narrative review," Biology, vol. 10, no. 7. MDPI AG, Jul. 01, 2021. doi: 10.3390/biology10070644.

[25] Y. Zhou et al., "Development of a Nursing Skill Training System Based on Manipulator Variable Admittance Control," in IEEE/ASME International Conference on Advanced Intelligent Mechatronics, AIM, Institute of Electrical and Electronics Engineers Inc., 2023, pp. 1226–1231. doi: 10.1109/AIM46323.2023.10196280.

[26] N. Hogan, "Impedance control: An approach to manipulation," in 1984 American control conference. IEEE, 1984, pp. 304–313.

[27] H. Maithani, J. A. C. Ramon and Y. Mezouar, "Predicting Human Intent for Cooperative Physical Human-Robot Interaction Tasks," 2019 IEEE 15th International Conference on Control and Automation (ICCA), Edinburgh, UK, 2019, pp. 1523-1528, doi: 10.1109/ICCA.2019.8899490.

[28] Gadringer, S., Gattringer, H., and Mueller, A.: Assessment of force control for surface finishing – an experimental comparison between Universal Robots UR10e and FerRobotics active contact flange, Mech. Sci., 13, 361–370, https://doi.org/10.5194/ms-13-361-2022, 2022.